Materials Chemistry and Physics 325 (2024) 129737

Contents lists available at ScienceDirect

Materials Chemistry and Physics

journal homepage: www.elsevier.com/locate/matchemphys

Poly(ethylene terephthalate) glycol/carbon black composites for 4D printing

Davood Rahmatabadi [a], Abbas Bayati [a], Mahdi Khajepour [a], Kiandokht Mirasadi [a], Ismaeil Ghasemi [b], Majid Baniassadi [a], Karen Abrinia [a], Mahdi Bodaghi [c,*], Mostafa Baghani [a,**]

[a] School of Mechanical Engineering, College of Engineering, University of Tehran, Tehran, Iran
[b] Faculty of Processing, Iran Polymer and Petrochemical Institute, Tehran, Iran
[c] Department of Engineering, School of Science and Technology, Nottingham Trent University, Nottingham, NG11 8NS, UK

HIGHLIGHTS

- Development and 4D printing of PETG-CB shape memory polymer composites.
- PETG-CB composites exhibit over 97 % shape recovery rate in shape memory tests.
- 1 % CB composite demonstrates optimal tensile strength and shape memory properties.
- SEM analysis confirms uniform CB particle distribution in PETG matrix.
- Enhanced mechanical properties observed with carbon black addition to PETG.

GRAPHICAL ABSTRACT

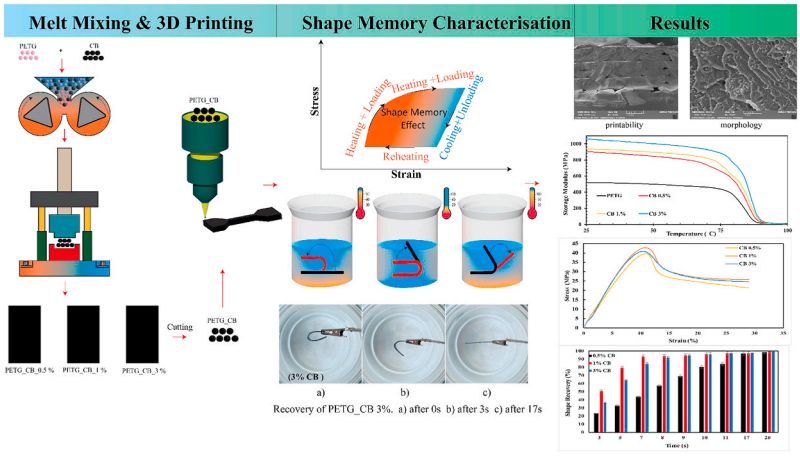

ARTICLE INFO

Keywords:
4D printing
PETG-CB composites
Shape memory polymers
Fused deposition modeling (FDM)
Nanocomposites
Mechanical properties

ABSTRACT

This research introduces PETG-CB (poly(ethylene terephthalate) glycol modified with carbon black) composites, a new class of shape memory polymers 4D printed using the Fused Deposition Modeling (FDM) method. Nanocomposites with varying concentrations of CB (0.5 %, 1 %, and 3 % by weight) are developed to enhance the functional performance of PETG in 4D printing applications. Comprehensive characterization at the micro- and macro-scale, including dynamic thermal mechanical analysis (DMTA), scanning electron microscopy (SEM), and mechanical testing, is employed to assess the viscoelastic behavior, microstructural integrity, and mechanical strength under thermal stimulation. Experimental results reveal that CB addition significantly alters the glass transition temperature and improves mechanical properties, with the 1 % CB composite demonstrating optimal tensile strength and enhanced shape memory effects. SEM analysis confirms a uniform distribution of CB

* Corresponding author.
** Corresponding author.
E-mail addresses: mahdi.bodaghi@ntu.ac.uk (M. Bodaghi), baghani@ut.ac.ir (M. Baghani).

https://doi.org/10.1016/j.matchemphys.2024.129737
Received 3 May 2024; Received in revised form 10 July 2024; Accepted 16 July 2024
Available online 17 July 2024

particles, contributing to the improved mechanical properties and printability of the nanocomposites. The shape memory tests show excellent recovery rates above 97 %, with faster recovery observed in composites with higher CB content. These findings highlight the potential of PETG-CB composites in applications requiring rapid response and high mechanical performance, making them promising materials for future advancements in the 4D printing technology.

1. Introduction

Additive manufacturing, also known as three-dimensional (3D) printing, is one of the most advanced manufacturing technologies [1]. It involves producing 3D structures using a computer-aided design (CAD) file by applying materials layer by layer [2]. The range of materials that can be used in this process includes polymers, metal alloys, ceramics, and composites [3]. Compared to traditional manufacturing methods, this technology offers advantages such as the ability to design complex structures, cost-effectiveness, and the ability to save raw materials [4]. While 3D printing has transformed the manufacturing industry by enabling rapid prototyping and production of complex geometries, it still faces several limitations that necessitate the development of 4D printing technologies [5]. One significant limitation of 3D printing is its inability to address the issue of shape memory and self-healing materials [6,7]. 3D-printed parts are often rigid and cannot change shape or adapt to changing conditions, which can limit their functionality and durability. In contrast, 4D printing enables the creation of systems that can change shape in response to temperature, light, or other environmental stimuli [8,9]. For example, it is possible to create biomedical devices that can change shape in response to body temperature or pH levels [10]. Similarly, aerospace components can be developed that adapt to changing conditions, such as solar cells of a satellite that can change shape in response to sunlight [11]. Additionally, smart textiles can be created that adjust their shape or stiffness in response to environmental conditions, such as clothes that can change texture in response to temperature or humidity [12].

In the meantime, shape memory polymers (SMPs) due to the cheapness of their printing mechanism, better Shape Memory Effect (SME), the possibility of changing and adjusting mechanical, physical and shape memory properties (adding sensitivity to different and multiple stimuli at the same time) and high plasticity and biocompatibility have attracted the most attention in the field of 4D printing. SMPs can alter their shape over time when exposed to external stimuli in the form of heat [13], electric field [14], magnetic field [15], light [16], or pH [17]. These features makes SMPs highly promising for various applications, including sensors and actuators [18], as well as the development of intelligent medical devices [19].

Among the various 3D printing techniques, the Fused Deposition Modeling (FDM) method is considered the most widely used method due to its ease and lower cost [20]. In this method, thermoplastic polymers are used as raw materials. These materials are extruded through a nozzle layer by layer based on the designed digital file and connected to create a 3D object [21]. One of the advantages of FDM 3D and 4D printing is cheap and recyclable thermoplastics, although due to the low strength of mechanical properties and poor stiffness, most materials need to be reinforced [22].

Amorphous Poly(ethylene terephthalate) glycol, also known as PETG, is a versatile filament often used in 3D printing. Recently, researchers have taken an interest in this transparent material due to its high extrusion printing capability [23]. In a study by Soleyman et al. [24], the SME and 4D printing capability of PETG were investigated. The results showed that PETG has an excellent SME with a shape recovery rate of over 96 %. Subsequent studies [25] looked at the effect of programming temperature on PETG 4D printing samples and found that increasing the programming temperature reduces the shape recovery ratio, while increasing the shape fixity ratio. Another study conducted by Aberoumand et al. [23] focused on the self-forming ability of PETG 4D printed samples. They also examined the impact of planning conditions and printing parameters on self-forming behavior. They found that lower printing temperatures and higher printing speeds improve the self-bending and shape recovery ability of the printed parts. Summary of these results showed that PETG is a SMP with high SME in different modes and temperatures with high deformation. These features, together with the excellent printing ability, put PETG next to Poly(lactic acid) (PLA) as the most widely used pure commercial SMP for 4D printing by FDM. Because thermoplastics do not have strong crosslinks (hard points), they mostly require strengthening this part. Usually, to achieve more favorable SME, two methods of strengthening are used by blending or synthesizing of a new SMP. The additional operation to enhance the SME is accompanied by many complications, and this problem is aggravated by considering the challenges of 3D printing of new materials. Therefore, PLA and PETG can be mentioned as the only pure SMP with excellent printability.

Due to the unique features and numerous applications of PLA, solving the issue of brittleness and low formability of PLA has been one of the key areas of focus in the field of 3D and 4D printing, and its softening with different thermoplastic elastomers (TPEs) has been done in recent years [26]. Rahmatabadi et al. [27] used the FDM method to uniformly mix thermoplastic polyurethane (TPU) with PLA, 3D printed the blends, and found that higher TPU content led to decreased strength but increased flexibility in the blends. These results indicate that adjusting the TPU content can modify the mechanical properties of PLA-TPU blends. Sangeetha et al. [28] conducted a study to investigate the effects of using Styrene Ethylene Butylene Styrene (SEBS) block co-polymer as a toughening agent on the toughness, strength, and heat resistance of PLA. Based on reviewed literature, it has been found that pure PLA exhibits significant brittleness. Therefore, for 4D printing applications that require enhanced mechanical properties through the addition of fillers, strengthening the plasticity of PLA through impregnation with TPEs becomes necessary. Furthermore, due to the low strength of 3D printed parts by FDM, it is necessary to strengthen the mechanical properties, and the use of carbon-based fillers to strengthen the mechanical properties of PLA requires the use of plasticizers and TPEs.

In contrast, PETG demonstrates high plasticity at ambient temperature, allowing the addition of fillers without the need for TPEs, thereby improving its mechanical properties [25]. The shape memory potential of PETG copolymer is promising, though its mechanical properties, specifically tensile strength, require further enhancement. The ability to cold program and high formability at ambient temperature distinguishes PETG from PLA [21,25]. In addition, PETG, unlike PLA, can be reinforced with carbon black without the need for softening and blending with TPEs. Carbon black (CB) is a widely utilized reinforcing filler within the rubber industry, offering significant improvements to tensile strength, elasticity modulus, and compressive strength.

In this investigation, we meticulously explore the capabilities of PETG-CB composites across varying concentrations of carbon black (0.5 %, 1 %, and 3 %) tailored for 4D printing using the FDM method. This research aims to systematically assess the mechanical and shape memory properties of these composites when subjected to thermal stimulation, offering a novel insight into their adaptability and resilience. By employing advanced techniques such as dynamic thermal mechanical analysis (DMTA) and scanning electron microscopy (SEM), we not only verify the enhanced thermal properties but also scrutinize the printing dynamics and morphological characteristics of the printed composites.

The outcomes of this study are poised to make substantial contributions to the advancement of 4D printing technology, showcasing the potential of PETG-CB composites to revolutionize applications that require materials with superior mechanical robustness and dynamic performance capabilities. Our findings underscore the potential of integrating carbon black with PETG, setting a new benchmark for the design and development of next-generation smart materials.

2. Materials and methods

2.1. Materials

For the preparation of PETG-CB nanocomposites, we used a 1.75 mm diameter PETG filament manufactured by eSUN (Shenzhen, China) and carbon black nanoparticles (CB) manufactured by fine nano. The PETG filament was first crushed into granules using a plastic grinder. Additionally, the granules were dehumidified in an oven at a temperature of 60 °C.

2.2. Processing of PETG-CB nanocomposites

PETG-CB nanocomposites were prepared through a melt mixing method using a Brabender internal mixer made in Germany. Three different concentrations of CB nanoparticles, 0.5 %, 1 %, and 3 %, were employed. First, PETG granules were melted inside the mixer at 200 °C and a speed of 60 rpm for 2 min. Following this, CB nanoparticles were added to the molten PETG. The mixture was kept inside the machine for 10 min to ensure a uniform distribution of the nanoparticles in the polymer field. The output material was obtained in a lump form, which was further processed using a press machine. A hot press with a temperature of 200 °C and a cold press with a pressure of 60 kPa were used to convert the lumps into thin sheets with a thickness of 1 mm. The resultant thin sheets were then transformed into granules. The schematic of the steps of producing PETG-CB composites and converting them into sheets and then granules is presented in Fig. 1.

2.3. 3D printing

In this study, the Chakad CSS1 printer manufactured in Iran was utilized to flawlessly 3D print PETG-CB nanocomposites. According to Fig. 2, by melting the granular materials within its thermal chamber, the printer effectively eliminated the requirement for filament removal. The melted materials were then directed to the nozzle through air pressure to initiate the printing process. This direct granule-based printing mechanism can be very useful for 3D printing of composites containing a high weight percentage of reinforcement. In addition, the use of a pneumatic system helps to provide the ability to continuously control and manipulate the output melt flow and avoid clogging of the nozzle and disconnection and connection of the flow. Table 1 lists the FDM printing parameters used to process the nanocomposites in this study.

2.4. Characterization

2.4.1. DMTA and MFI

DMTA is a technique used to identify the viscoelastic properties of polymers. This process involves applying an oscillating force on a sample and analyzing the material's response to that force. In this research, a Mettler Toledo dynamic thermomechanical device manufactured in Switzerland was utilized. The test was conducted in the temperature range of 25 °C–100 °C, at a constant frequency of 1 Hz, and under a three-point bending load. Also, to evaluate the rheological behavior of the extruded material and its effect on printability, the Melt Flow Index (MFI) was calculated for about 10 g of pure PETG and all three composites granules at the printing temperature (200 °C) with a weight of 2.16 kg according to the ASTM D1238 standard.

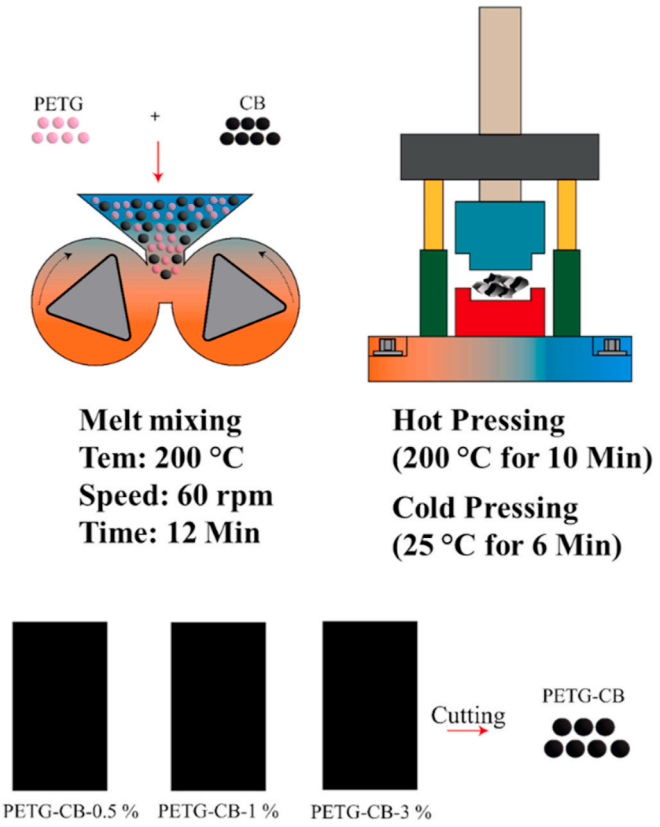

Fig. 1. Schematic of different manufacturing stages PETG-CB composites and preparing granules for 3D printing.

2.4.2. Microstructure evaluation

SEM analysis is used to image samples and determine their surface characteristics, including morphology, component compatibility, and print quality. In this study, the Vegall device, manufactured by Tescan, was used to image the samples. To reduce the brittleness of the samples, they were first immersed in liquid nitrogen and then broken. The fracture surface of the samples was covered with gold to improve image quality.

2.4.3. Mechanical properties

The mechanical properties of the material were assessed through a uniaxial tensile test, utilizing the Santam machine. To ensure precise results, the test was repeated three times for each dog bone sample, following the ASTM D638 type V standard at room temperature. The displacement speed was set to 3 mm/min, and the load cell was calibrated at 100 kg.

2.4.4. Shape memory effect

The shape memory properties of 3D printed PETG-CB composites were thoroughly evaluated using the shape memory cycle. According to Fig. 3, this cycle consists of two stages: shape programming and shape recovery. By applying heat exceeding the glass transition temperature of the polymer, a specific strain was created in the part, based on the loading mode. Upon reducing the temperature, the sample stored the strain, and the stabilized strain-to-applied strain ratio was measured as the shape fixity parameter. The final stage of this cycle involved heating the samples again, enabling them to regain their original shape. This resulted in the ratio of the recovered strain to the stabilized strain, known as the shape recovery parameter. The programming and shape recovery stages were conducted using the bending loading mode in both water at a temperature of approximately 100 °C. The heating and cooling time of the first stage was estimated to be 60 s. The parts'

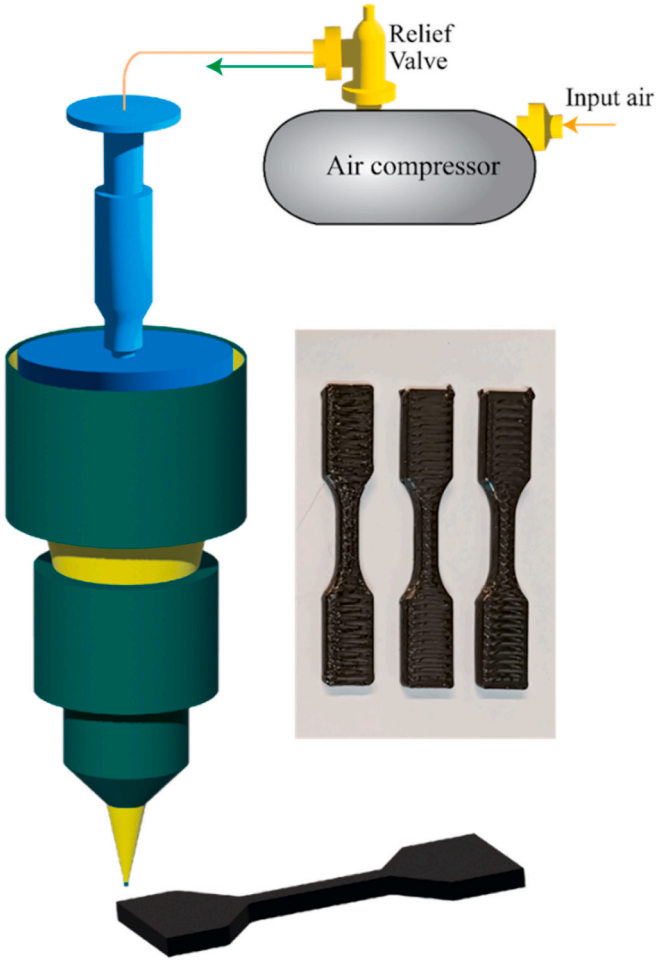

Fig. 2. Schematic of direct granule-based 3D printer and printed parts.

Table 1
Variable parameters in 3D printing by FDM method of PETG-CB nanocomposites.

Printing Parameters	Values
Velocity (mm/min)	300
Nozzle Temperature (°C)	200
Bed Temperature (°C)	45
Nozzle Diameter (mm)	0.6
Layer Thickness (mm)	0.4
Printing Direction	0/90
Air pressure (Bar)	3–5 bar

geometry was considered as a beam with dimensions of 4 × 1 cm and a thickness of 1 mm. Shape memory performance was measured based on Fig. 3.

3. Results and discussion

3.1. DMTA

Fig. 4 illustrates the dynamic mechanical thermal analysis conducted on neat PETG and its nanocomposites containing varying amounts of carbon black (0.5 %, 1 %, and 3 % by weight). This analysis serves as a valuable method for assessing the viscoelastic behavior of materials across different temperatures [29]. Understanding the viscoelastic behavior of materials across different temperatures is essential for analyzing the shape memory properties of the material [30]. The test measures how the materials respond to cyclic stresses, such as sinusoidal

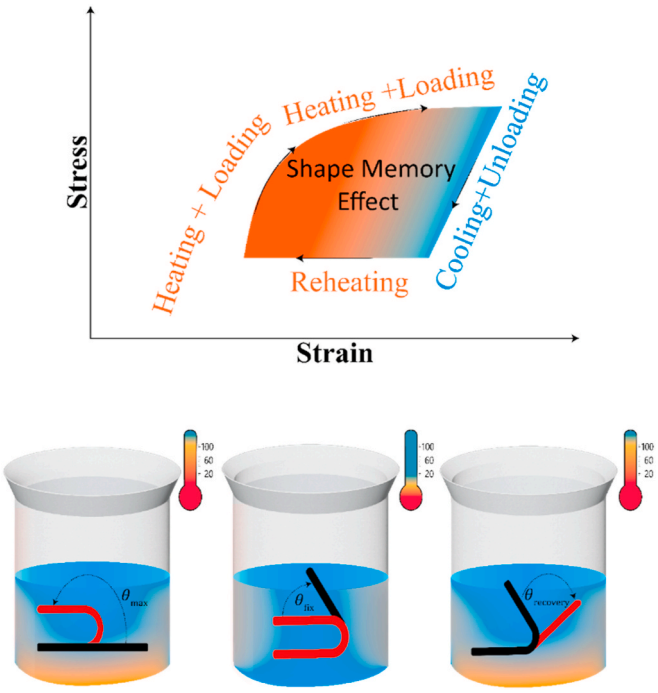

Fig. 3. Schematic explanation of shape memory cycle.

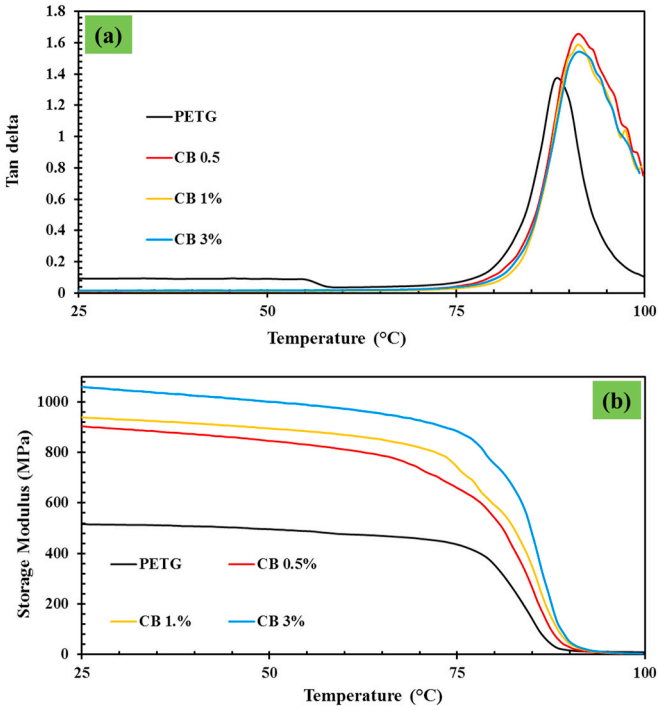

Fig. 4. DMTA results for neat PETG and its nanocomposites.

forces, under different temperature conditions [31].

In viscoelastic materials, the response to an applied force can be characterized by two components: the elastic response (represented by the storage modulus, E′) and the viscous response (represented by the loss modulus, E′′) [32]. The elastic response reflects the reversible deformation of the material akin to a spring-like behavior, while the viscous response indicates the dissipation of energy within the material resembling a damper-like behavior. Viscous responses arise from factors like molecular movement, intermolecular friction, and heat generation

mechanisms, especially in the segmental motion within the solid state [33]. The ratio of the loss modulus to the storage modulus, known as Tan δ, quantifies the material's damping ability. This parameter helps in gauging how effectively the material dissipates energy in response to applied stresses.

Fig. 4 (a) depicts the change in tan δ as a function of temperature for pure PETG and its nanocomposites. Peaks on the tan δ versus temperature graph indicate transitions in the material's state. The most significant peak in tan δ diagram signifies the transition from a glassy state to a rubbery state, occurring at the glass transition temperature (Tg) of the material [34]. These transitions, particularly the glass-rubber transition, are integral to the material's shape memory behavior because the temperature at which these transitions take place serves as the switching temperature for shape recovery.

As the temperature rises, the free volume within the material increase, leading to a higher degree of movement among the molecular chains in the non-crystalline section. This eventually results in the emergence of the glass transition [35]. It is observed that the peak for pure PETG appears around 85 °C. With the addition of 0.5 % carbon black, this temperature noticeably shifts to approximately 93 °C. Further additions of carbon black have a diminishing effect on Tg. Specifically, the introduction of 1 % and 3 % carbon black increases the Tg to 94 °C and 95 °C, respectively.

The glass transition temperature (Tg) is associated with the polymer's chain mobility. Greater chain mobility leads to increased flexibility and a lower Tg of the material. Incorporating carbon black nanoparticles into PETG elevates the Tg due to their ability to restrict the mobility and flexibility of the polymer chains. Consequently, this restriction results in a more rigid behavior of the material and a higher Tg. The extent of Tg change is influenced by the interaction between the polymer and the filler material [36]. At lower concentrations of carbon black, a significant increase in Tg compared to pure PETG is observed due to the pronounced restriction effect on polymer chains. However, with higher concentrations of carbon black, the likelihood of agglomeration increases, resulting in diminished interactions between the polymer and particles. This leads to a lesser increase in Tg.

It is noticeable that when carbon black is added to PETG, the height of tan δ increases compared to pure PETG. This indicates that the ratio of the loss modulus to the storage modulus increases, showing that the material exhibits more damping behavior rather than elastic behavior. This change is due to the interaction between the polymer and particles, leading to a more viscous behavior of the material. The increased damping behavior of the material with the addition of nanoparticles is also explained by Suhr et al. [37]. Consider a single nanoparticle embedded within the polymer matrix, experiencing deformation as depicted in Fig. 5 under a uniaxial load. The energy dissipation (ΔW) resulting from the interfacial slippage of this nanoparticle can be quantified using Equation 1.

$$\Delta W = \int \tau_{cr}\,(\delta u) dS$$

where τ_{cr} is the critical interfacial shear stress, δu is the slipping distance, and dS is the active area of the filler that participates in the sliding. When normal and shear stresses are applied to the particle, the normal stress causes significant separation between the nano particle and the matrix. As a result, the contact between the matrix and the particle becomes linear.

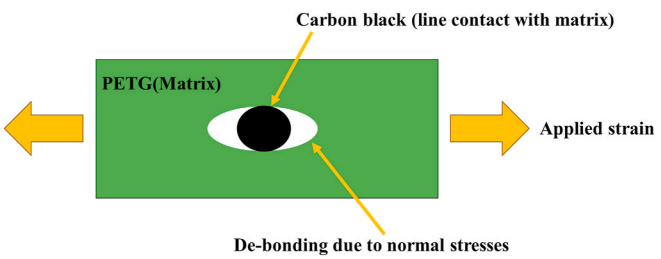

Fig. 5. Schematic of deformation profile around a nanoparticle (adopted from Ref. [37]).

When nano particles are added to the polymer matrix, it increases the active interfacial contact area (dS) and contributes to interfacial slippage. According to equation 2, this increase in contact area leads to higher energy loss (ΔW) and consequently increases the damping of the material, which is reflected in the heightened tan δ. However, as the number of extra nanoparticles increases and these particles cluster together, the active interfacial contact area (dS) decreases, leading to reduced energy loss and damping. This decrease in damping is evident in the reduced height of the tan δ.

Fig. 4 (b) illustrates the variation of storage modulus across a temperature range of 25–100 °C. The Figure illustrates three distinct regions: a glassy region with a high storage modulus, indicating limited movement of polymer chains; a transition region where the storage modulus drops suddenly; and a rubbery region where the storage modulus remains constant with increasing temperature.

At room temperature, an increase in the concentration of nanoparticles correlates with a rise in the storage modulus. Moreover, composites containing higher levels of carbon black (CB) exhibit heightened rigidity within this temperature range. The viscoelastic properties of nanocomposites are influenced by factors such as filler content, the quality of bonding between filler and matrix, and the arrangement of the filler particles. Typically, the enhancement in storage modulus observed across various nanocomposites can be attributed to the interaction between the polymer matrix and the nanofillers, which restricts the mobility of the polymer chains [38].

In the rubbery region, it is observed that all nanocomposites behave similarly to neat PETG at higher temperatures and beyond the glass transition temperature. This indicates that the addition of nanoparticles does not significantly alter the mechanical behavior of the material in this phase.

3.2. MFI and printability

MFI of a thermoplastic material is a measure of how easily it flows when melted and subjected to a specific temperature and pressure. It is defined as the amount of material that flows through a small opening in 10 min. The MFI is an important indicator of a material's flowability [39]. The material extrusion 3D printing process involves melting and extruding material. Direct pellet printing, is very similar to MFI testing. In both processes, a syringe-like mechanism is used to push the melted material through a small opening. Because of this similarity, the MFI test can help us understand how a material behaves when it's melted and how it will behave during the direct printing process. However, to fully evaluate how well a material can be printed, we also need to consider other factors beyond just its melted behavior [40].

MFI for pure PETG and PETG-CB composites with weight percentage of 0.5 %, 1 % and 3 % were 7.34 ± 0.35, 7.16 ± 0.49, 7.03 ± 0.51 and 6.81 ± 0.63 g/10 min, respectively in printing temperature. It shows that MFI slightly decreases with the increase in the weight percentage of CB. The decrease in MFI with increasing CB content in nanocomposites has also been reported by other researchers for polyethylene compounds [41]. Furthermore, Shenavar et al. [42] investigated the flow and mechanical properties of carbon black-filled acrylonitrile butadiene styrene (ABS) and found that MFI decreases with increasing CB content.

It is expected that better flowability of neat PETG can result in better printability compared to CB-filled counterparts. MFI decreasing trend can be attributed to the high surface activity of CB particles, which causes significant hydrodynamic interaction, leading to an increase in flow resistance between the sliding layers of molten material. Additionally, nanoparticles restrict the free movement of polymer chains within the melt, decreasing flowability. However, these effects are

minimal in low-content CB composites. As evident from the data, the variation of MFI with carbon black content is very small. It is noticeable that with the addition of 3 % CB, the MFI varies only by about 7 % compared to neat PETG. Moreover, it has been shown by reserachers that increasing pressure in the MFI test also increases MFI [42]. Similarly, in direct pellet printing processes, the flow of melted material can be regulated and increased by adding pneumatic pressure. The small variation in composite MFI can be disregarded by increasing air pressure slightly during the printing process.

Fig. 6 shows the SEM images of the fracture section of pure PETG and PETG-CB composites 3D printed by the material extrusion method. The rasters, layered structure and triangular microholes in SEM images for PETG and all three PETG-CB composites are clearly visible, which are characteristics of 3D printed parts. These characteristics can be strongly or weakly displayed according to the physical properties and printing ability of the material. In materials with suitable rheological properties and uniform morphology, the volume of microholes can be smaller and the quality of the layers' connection can be stronger. According to Fig. 6, the connection in the interfaces and between the layers and grids is stronger for pure PETG, but the connection of the layers and the density of triangular microholes are almost the same for all three composites. Based on the images in Fig. 6(a–c), although PETG is also a material with good printing ability, it still has triangular microholes. The exit of the melt from the spherical nozzle causes grids with a circular cross-section to be placed together and the gap between these grids creates triangular holes that can be seen in all samples. This problem can be reduced by increasing the output flow and integrating the grids into each other or increasing the temperature of the nozzle to flow more melt. The presence of carbon-based fillers decreases the MFI of the melt and in this way can contribute to the increase of micropores. In addition, the increase in weight percentage of CB is another factor to reduce printability. With the increase of CB fillers, which remain unchanged in the molten polymer at the printing temperature, the possibility of nozzle clogging increases greatly, and by cutting and connecting the output flow, it can destroy the connection of the layers and increase the empty space. The only positive point of adding CB fillers in terms of printability is reducing the shrinkage coefficient of composites, which prevents the reduction of the cross-sectional area and the weakening of the bonding interface of the grids. The addition of CB, with much lower shrinkage and thermal sensitivity compared to the polymer matrix, improves the bonding quality of layers and printability. This issue can be the reason for the improved printability for the composite containing more CB (Fig. 6 (j)–(l)).

In addition, other factors play a role in the high printing ability of all three PETG-CB composites. Using the optimal volume percentage of CB and the proper mixing method, in addition to achieving a uniform morphology and proper distribution of the filler, improves printability and mechanical properties. CB fillers with spherical geometry is the best option for strengthening the mechanical properties of 3D printed parts due to its ability to distribute and create better rheological properties, and it brings the least printing challenges, and allows the addition of high weight percentages. In addition to all the mentioned factors related to CB fillers and its distribution, the polymer matrix (PETG) and the printing mechanism used also play a fundamental role in achieving high printability. PETG is one of the most widely used commercial materials in this field due to its high printing ability. Using a pneumatic system to control, manipulate and strengthen the feeding system helps to create a stable output flow, so that the it can be continuously controlled, and in case of clogging of the nozzle or reduction of the output flow by increasing the air pressure, the disruption of the output flow should be prevented. For this reason, increasing the weight percentage of CB fillets has not affected the printing ability.

3.3. Morphology

In Fig. 7, the morphology and distribution of CB in the PETG matrix in three different weight percentages are presented. According to Fig. 7 (a)–(c), the composite containing 0.5 % by weight CB has a uniform distribution of fillers and a uniform structure is observed. The use of melt mixing method with application of high shear stress, almost low volume and spherical geometry of CB fillers is one of the factors of uniform distribution in this composite. According to Fig. 7 (d)–(f), with the doubling of the weight percentage of the fillers, uniform distribution is still observed in the polymer matrix. The presence of tracks of CB in all composites (even the composite containing 0.5 % by weight) can be due to the mechanism of material extrusion 3D printing. The flat and smooth fracture surfaces for the composite containing 0.5 % and 1 % by weight of CB can be seen in Fig. 7 (a) and (d), indicating a lower filler-matrix interface. In the composite containing 3 % by weight of CB, the uneven fracture surfaces and the accumulation of fillers is observed in some areas.

In composites containing filler, several other factors affect morphology, printability and ultimately mechanical properties. Weight percentage, geometry, filler distribution and filler-matrix bonding are four important factors in polymer matrix composites to achieve desired properties. The presence of filler in the polymer matrix increases the mechanical properties due to its higher strength and hardness, but the relationship between the weight percentage of the filler and the mechanical properties of composite is not direct, and the optimal mechanical properties are achieved at a specific weight percentage of the filler, and this weight percentage is determined by other factors. Proper filler distribution is the most important factor in achieving optimal mechanical properties. Increasing particles up to a certain weight percentage can achieve a homogeneous and balanced structure, and with excessive increase of particles, non-uniform morphology with agglomerate areas increases. These accumulation areas of filler are the source of crack propagation and growth due to high porosity and lack of strong strength. The geometry of the filler is also effective in determining the optimal volumetric value of the filler in the polymer matrix, and fillers with spherical geometry have a larger volume to proper distribution and prevent agglomeration.

3.4. Mechanical properties

Results from tensile tests conducted on 3D printed pure PETG and PETG-CB composites, as depicted in Fig. 8, provide valuable insights. The stress-strain graphs reveal a significant observation: as the quantity of CB increases, there is a noticeable ascent in the slope during the linear phase of the curves. This finding indicates a positive correlation between CB quantity and mechanical strength. Remarkably, the composite PETG-CB-1% stands out by peaking at tensile strength among the tested variants. In fact, the upward trend of the tensile strength and the slope of the linear region continues until the composite containing 1 % CB, and with the increase of the amount of CB to 3 %, the tensile strength and the slope of the linear region decrease. This outcome underscores the potential for enhancing the mechanical properties of PETG-based composites through controlled CB incorporation. The interaction between various factors influences the tensile strength and elongation of nanocomposites. Beyond nanoparticle concentration, factors like distribution and filler-polymer matrix bonding play vital roles. Additionally, the 3D printing process introduces porosity and shrinkage, impacting part quality. Consequently, the relationship between tensile strength, elongation, and filler weight percentage is nonlinear due to these intricate interactions.

The p-value calculated for Ultimate Tensile Strength (UTS) was 0.003, which indicates high significance. A p-value of 0.05 or lower is generally considered statistically significant. The data depicted in Fig. 9 illustrates the behaviour of elongation and strength during a uniaxial tensile test until the UTD point. Notably, there's a fluctuation in tensile strength, ranging from 37.19 MPa to 42.69 MPa. The highest strength is observed for PETG-CB-1%, reaching 42.69 MPa, which has increased by 14.8 % compared to pure PETG. Increasing the weight percentage of CB

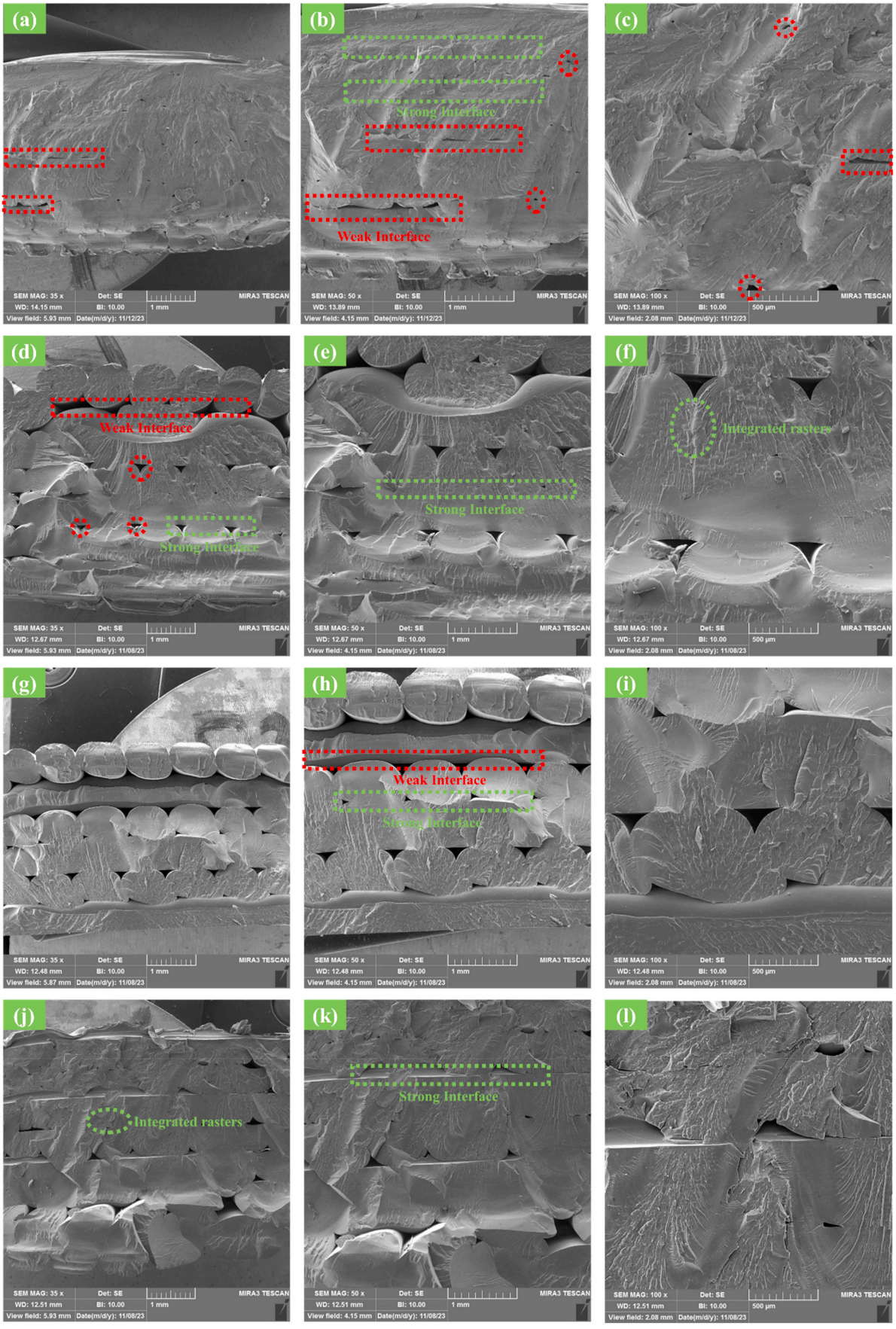

Fig. 6. SEM images to check the printability of: (a–c) pure PETG and PETG-CB composites containing: (d–f) 0.5 %, (g–i) 1 % and (j–l) 3 % carbon black.

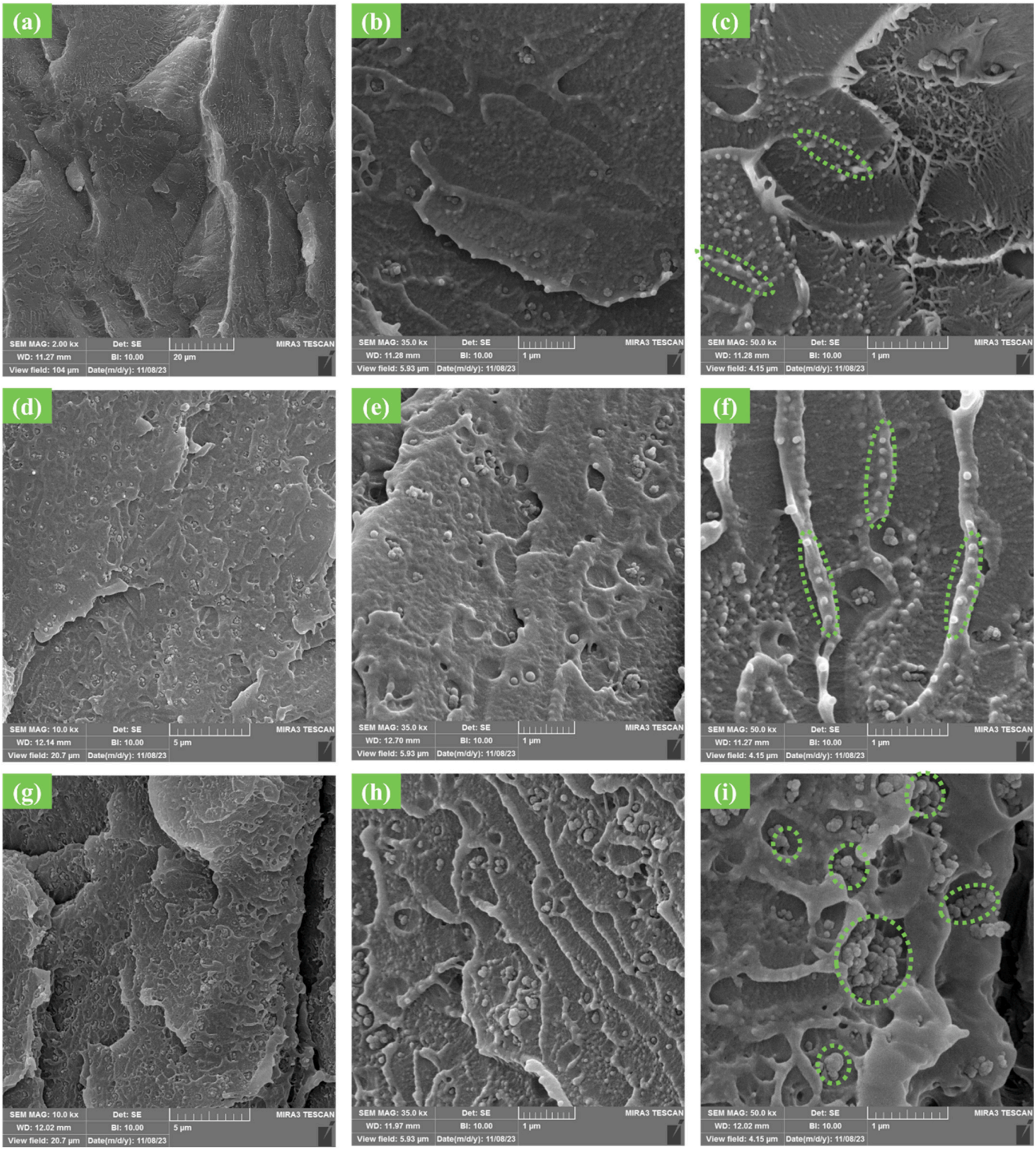

Fig. 7. Morphology of 3D printed PETG-CB composites containing: (a–c) 0.5 %, (d–f) 1 % and (g–i) 3 % carbon black.

from 0.5 % to 1 % enhances strength, but further increment to 20 % reverses this trend, reducing strength to 40.74 MPa. SEM results indicate that higher CB concentrations adversely affect 3D printing quality and nanoparticle dispersion within PETG-CB composites. Specifically, the PETG-CB-3% composite exhibits significant nanoparticle agglomeration, likely leading to crack initiation and stress concentration, thus compromising mechanical properties. Moreover, increased nanoparticle content and agglomeration elevate melt viscosity during printing, hindering melt flow regulation and resulting in increased porosity and weaker bonding between printed layers and grids. These factors collectively contribute to the strength diminishment of PETG-CB nanocomposites with higher nanoparticle content.

The toughness values for the 3D printed pure PETG and PETG-CB nanocomposite up to the UTS threshold and at 30 % strain are depicted in Fig. 10. These values are determined by calculating the area under the stress-strain curves, reflecting a trend similar to the variations in

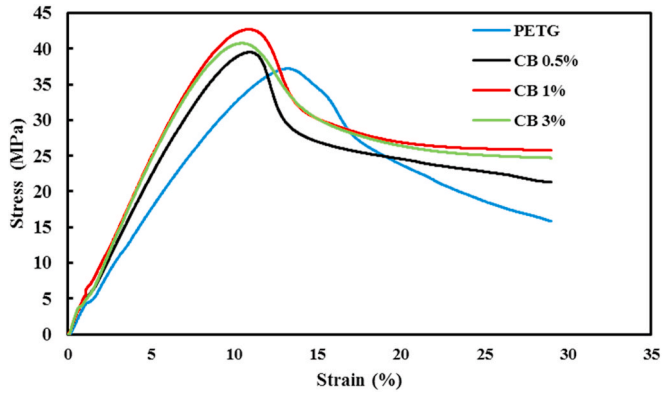

Fig. 8. Stress-strain diagrams for printed pure PETG and PETG-CB composites.

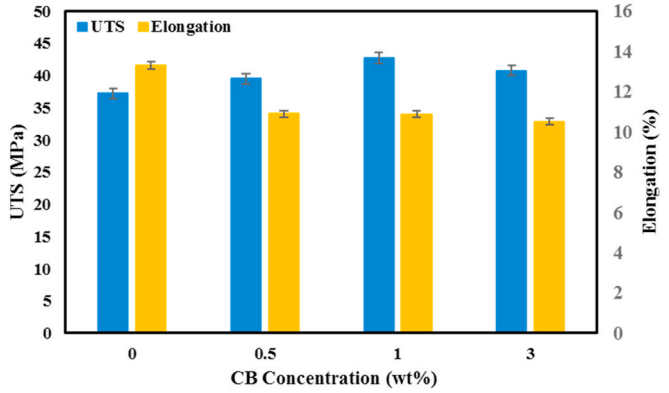

Fig. 9. Variations of UTS and elongation for 3D printed pure PETG and PETG-CB composites in terms of weight percentage of carbon black.

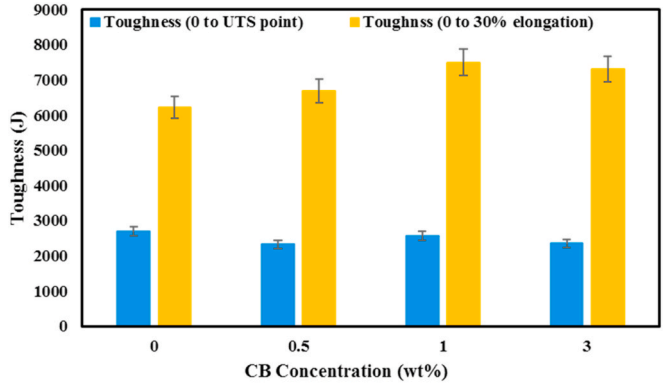

Fig. 10. Variations of toughness for 3D printed pure PETG and PETG-CB composites in terms of weight percentage of carbon black.

mechanical properties. Specifically, the pure PETG nanocomposite exhibits the lowest toughness at 6223J, attributed to its stress level, while PETG-CB composites according to the increase in weight percentage of CB show identical values at 6690J, 7499J and 7298J, respectively.

3.5. SME

The ability of 4D printed PETG-CB composites to recover their original shape when exposed to heat was tested by immersing them in boiling water to ensure they reached their glass transition temperature (Tg), which was determined through dynamic mechanical thermal analysis (DMTA). To assess the shape recovery of the 4D printed composites, a digital camera was employed to capture frames from a video showing the shape recovery process at different time intervals, as depicted in Fig. 11.

It is noteworthy that all the PETG-CB composites exhibited outstanding shape fixity, with values surpassing 95 %, which can be attributed to the substantial contrast in storage modulus before and after reaching the glass transition temperature (Tg). This discovery aligns with previous reports concerning neat PETG [24]. Another significant observation is that all the composites are able to recover their permanent shape in under 20 s, indicating a short recovery time, thus rendering these composites suitable for swift-response applications, such as rapid actuators.

Fig. 12 presents the shape recovery outcomes for pure PETG and PETG composites with varying CB concentrations. It is clear that both pure PETG and all the PETG-CB composites exhibited exceptional shape recovery, with a recovery rate exceeding 97 %. Specifically, composites containing 1 % and 3 % CB concentrations achieved 100 % shape recovery, while the pure PETG and composite with 0.5%wt CB achieved 97 % and 98 % shape recovery. The enhancement in shape recovery is caused by the formation of a physical network through the introduction of CB, which supplies extra entropic elasticity that helps restore specimens during the shape memory test. The addition of a small amount of CB established a suitable balance between fixed and reversible domains in PETG [43]. This formation of a CB physical network led to an improvement in the shape memory property of the composites. Additionally, the presence of a higher concentration of CB may lead to improved heat transfer within the material, facilitating better response to the heat stimulation and thus resulting in more effective shape recovery.

The study's findings also suggest that the addition of CB influenced the shape recovery speed of the composites. Specifically, samples with 1 % CB showed faster shape recovery than those with 3 %, and 3 % showed faster recovery than those with 0.5 % and pure PETG. In fact, pure PETG and composite containing 0.5 % CB have almost the same performance in shape recovery rate, especially in the initial seconds. This suggests that relatively high dosages of CB, had a detrimental effect on the preservation of the shape memory effect by causing bad chain flexibility. Therefore, it's evident that the dosage of CB has a significant impact on the shape recovery speed and the overall shape memory properties of the composites.

4. Conclusion

This study provides a comprehensive evaluation of the effects of CB nanoparticle incorporation on the properties of PETG composites, showcasing their enhanced capabilities for 4D printing applications. The incorporation of CB significantly improves the mechanical and shape memory properties of PETG, with the 1 % CB concentration demonstrating the most favorable balance between enhanced strength and effective shape memory behavior. The experimental results reveal that these composites not only exhibit superior tensile strength but also achieve exceptional shape recovery rates, surpassing 97 %. This makes them particularly suitable for applications requiring rapid and reliable responses to environmental stimuli. Furthermore, the research highlights the critical role of CB concentration in optimizing the viscoelastic and mechanical properties of the composites. While higher concentrations of CB lead to increased rigidity and potentially higher functional performance, they also introduce challenges such as particle agglomeration and increased porosity, which can adversely affect the print quality and mechanical integrity. The findings from this study underscore the potential of PETG-CB composites to revolutionize the field of 4D printing by providing materials that are not only mechanically robust but also exhibit dynamic, programmable behaviors suitable for a wide range of advanced applications. Future research should focus on exploring the long-term performance and environmental durability of these composites, as well as their practical implementation in industrial

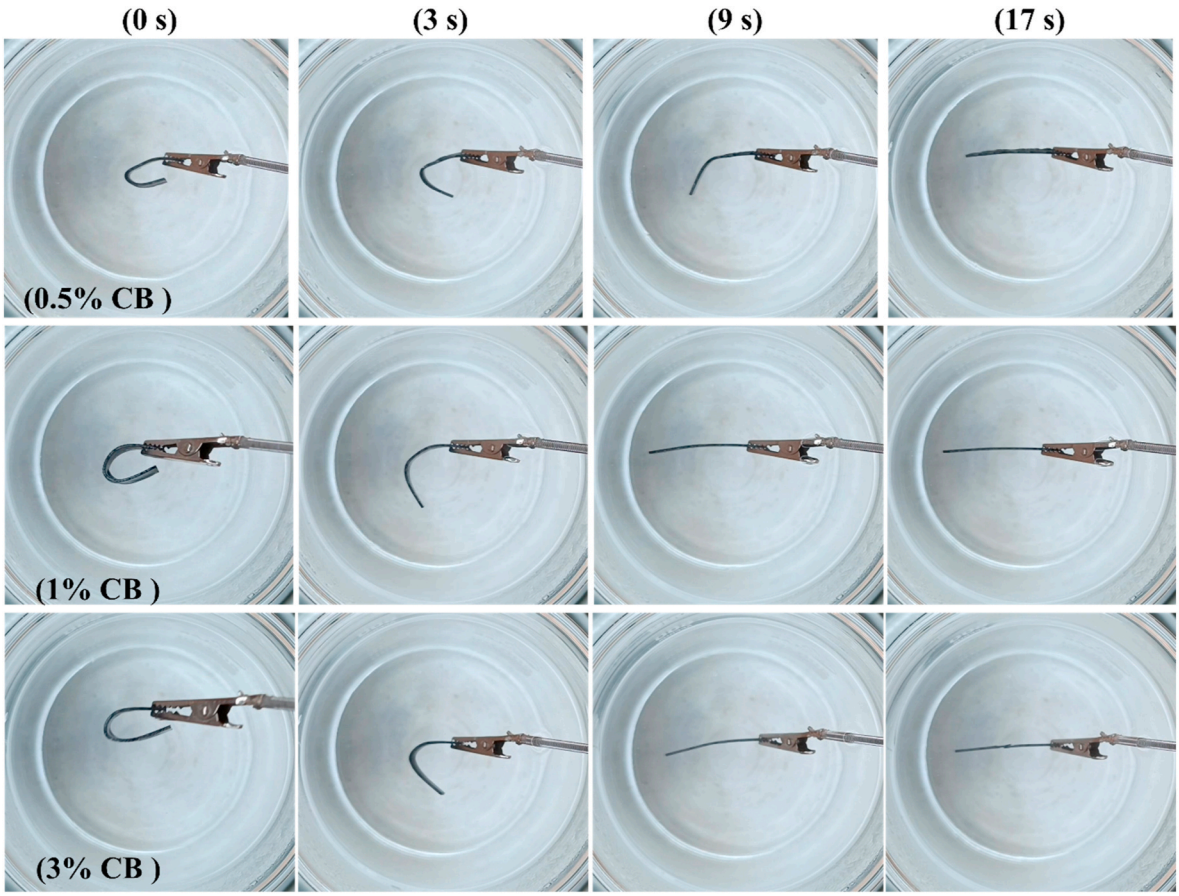

Fig. 11. Shape recovery process for PETG-CB composites at different time intervals.

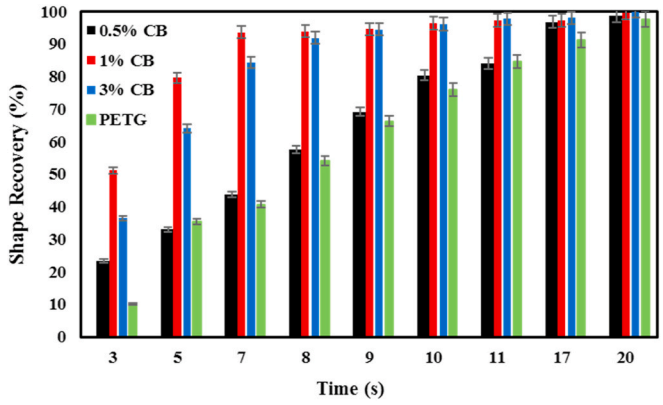

Fig. 12. Variations of shape recovery ratio for 3D printed pure PETG and PETG-CB composites in terms of time.

and biomedical applications.

CRediT authorship contribution statement

Davood Rahmatabadi: Writing – review & editing, Writing – original draft, Supervision, Methodology, Investigation, Formal analysis, Data curation, Conceptualization. **Abbas Bayati:** Writing – original draft, Visualization, Methodology, Investigation, Data curation. **Mahdi Khajepour:** Writing – original draft, Methodology, Investigation, Data curation. **Kiandokht Mirasadi:** Writing – original draft, Methodology, Investigation, Data curation. **Ismaeil Ghasemi:** Writing – review & editing, Supervision, Methodology, Investigation, Formal analysis, Conceptualization. **Majid Baniassadi:** Writing – review & editing, Supervision, Resources, Methodology, Investigation, Funding acquisition. **Karen Abrinia:** Writing – review & editing, Supervision, Methodology, Investigation. **Mahdi Bodaghi:** Writing – review & editing, Validation, Supervision, Methodology, Investigation, Formal analysis, Writing – original draft. **Mostafa Baghani:** Writing – review & editing, Supervision, Methodology, Investigation, Formal analysis.

Declaration of competing interest

The authors declare that they have no known competing financial interests or personal relationships that could have appeared to influence the work reported in this paper.

Data availability

Data will be made available on request.

Acknowledgement

Mahdi Bodaghi acknowledges the support by the Engineering and Physical Sciences Research Council (EPSRC) [grant number EP/Y011457/1].

References

[1] M.V. Varma, B. Kandasubramanian, S.M. Ibrahim, 3D printed scaffolds for biomedical applications, Mater. Chem. Phys. 255 (2020) 123642, https://doi.org/10.1016/J.MATCHEMPHYS.2020.123642.
[2] K. Sattari, Y. Wu, Z. Chen, A. Mahjoubnia, C. Su, J. Lin, Physics-constrained multi-objective bayesian optimization to accelerate 3d printing of thermoplastics, Addit. Manuf. 86 (2024) 104204, https://doi.org/10.1016/j.addma.2024.104204.

[3] S. Singh, S. Ramakrishna, R. Singh, Material issues in additive manufacturing: a review, J. Manuf. Process. 25 (2017) 185–200, https://doi.org/10.1016/j.jmapro.2016.11.006.
[4] A. Bayati, D. Rahmatabadi, I. Ghasemi, M. Khodaei, M. Baniassadi, K. Abrinia, M. Baghani, 3D printing super stretchable propylene-based elastomer, Mater. Lett. 361 (2024) 136075, https://doi.org/10.1016/J.MATLET.2024.136075.
[5] C. Yuan, T. Lu, T.J. Wang, Mechanics-based design strategies for 4D printing: a review, Forces Mech 7 (2022), https://doi.org/10.1016/j.finmec.2022.100081.
[6] A. Zolfagharian, H.R. Jarrah, M.S. Xavier, B. Rolfe, M. Bodaghi, Multimaterial 4D printing with a tunable bending model, Smart Mater. Struct. 32 (2023) 065001, https://doi.org/10.1088/1361-665X/ACCBA8.
[7] B.I. Oladapo, J.F. Kayode, J.O. Akinyoola, O.M. Ikumapayi, Shape memory polymer review for flexible artificial intelligence materials of biomedical, Mater. Chem. Phys. 293 (2023) 126930, https://doi.org/10.1016/J.MATCHEMPHYS.2022.126930.
[8] E. Soleyman, M. Aberoumand, D. Rahmatabadi, K. Soltanmohammadi, I. Ghasemi, M. Baniassadi, K. Abrinia, M. Baghani, Assessment of controllable shape transformation, potential applications, and tensile shape memory properties of 3D printed PETG, J. Mater. Res. Technol. 18 (2022) 4201–4215, https://doi.org/10.1016/J.JMRT.2022.04.076.
[9] R. Wang, C. Yuan, J. Cheng, X. He, H. Ye, B. Jian, H. Li, J. Bai, Q. Ge, Direct 4D printing of ceramics driven by hydrogel dehydration, Nat. Commun. 15 (2024), https://doi.org/10.1038/s41467-024-45039-y.
[10] C. Lin, Z. Huang, Q. Wang, Z. Zou, W. Wang, L. Liu, Y. Liu, J. Leng, Mass-producible near-body temperature-triggered 4D printed shape memory biocomposites and their application in biomimetic intestinal stents, Composites, Part B 256 (2023) 110623, https://doi.org/10.1016/J.COMPOSITESB.2023.110623.
[11] O. Testoni, T. Lumpe, J.L. Huang, M. Wagner, S. Bodkhe, Z. Zhakypov, R. Spolenak, J. Paik, P. Ermanni, L. Muñoz, K. Shea, A 4D printed active compliant hinge for potential space applications using shape memory alloys and polymers, Smart Mater. Struct. 30 (2021) 085004, https://doi.org/10.1088/1361-665X/AC01FA.
[12] H.L. Ornaghi, O. Bianchi, Temperature-dependent shape-memory textiles: physical principles and applications, Text 3 (2023) 257–274, https://doi.org/10.3390/TEXTILES3020017, 2023, Vol. 3, Pages 257-274.
[13] M. Aberoumand, K. Soltanmohammadi, D. Rahmatabadi, E. Soleyman, I. Ghasemi, M. Baniassadi, K. Abrinia, M. Bodaghi, M. Baghani, 4D printing of polyvinyl chloride (PVC): a detailed analysis of microstructure, programming, and shape memory performance, Macromol. Mater. Eng. 308 (2023) 2200677, https://doi.org/10.1002/mame.202200677.
[14] N.G. Sahoo, Y.C. Jung, N.S. Goo, J.W. Cho, Conducting shape memory polyurethane-polypyrrole composites for an electroactive actuator, Macromol. Mater. Eng. 290 (2005) 1049–1055, https://doi.org/10.1002/mame.200500211.
[15] A.M. Schmidt, Electromagnetic activation of shape memory polymer networks containing magnetic nanoparticles, Macromol. Rapid Commun. 27 (2006) 1168–1172, https://doi.org/10.1002/marc.200600225.
[16] H. Zhang, R. Zhang, C. Yuan, Modelling constrained recovery of UV-curable shape memory polymer toward 4D printing, Chem. Bioeng. (2024), https://doi.org/10.1021/CBE.4C00020.
[17] K. Strzelec, N. Sienkiewicz, T. Szmechtyk, Classification of shape-memory polymers, polymer blends, and composites, in: Adv. Struct. Mater., Springer Verlag, 2020, pp. 21–52, https://doi.org/10.1007/978-981-13-8574-2_2.
[18] M. Aberoumand, D. Rahmatabadi, K. Soltanmohammadi, E. Soleyman, I. Ghasemi, M. Baniassadi, K. Abrinia, M. Bodaghi, M. Baghani, Stress recovery and stress relaxation behaviors of PVC 4D printed by FDM technology for high-performance actuation applications, Sensors Actuators A Phys 361 (2023) 114572, https://doi.org/10.1016/J.SNA.2023.114572.
[19] Y. Wu, C. Su, S. Wang, B. Zheng, A. Mahjoubnia, K. Sattari, H. Zhang, J. Meister, G. Huang, J. Lin, A photocured bio-based shape memory thermoplastics for reversible wet adhesion, Chem. Eng. J. 470 (2023) 144226, https://doi.org/10.1016/j.cej.2023.144226.
[20] V. Mazzanti, L. Malagutti, F. Mollica, FDM 3D printing of polymers containing natural fillers: a review of their mechanical properties, Polymers (Basel) 11 (2019), https://doi.org/10.3390/polym11071094.
[21] D. Rahmatabadi, I. Ghasemi, M. Baniassadi, K. Abrinia, M. Baghani, 4D printing of PLA-TPU blends: effect of PLA concentration, loading mode, and programming temperature on the shape memory effect, J. Mater. Sci. 2023 (2023) 1–17, https://doi.org/10.1007/S10853-023-08460-0.
[22] F. Wang, F. Luo, Y. Huang, X. Cao, C. Yuan, 4D printing via multispeed fused deposition modeling, Adv. Mater. Technol. 8 (2023) 2201383, https://doi.org/10.1002/admt.202201383.
[23] M. Aberoumand, K. Soltanmohammadi, E. Soleyman, D. Rahmatabadi, I. Ghasemi, M. Baniassadi, K. Abrinia, M. Baghani, A comprehensive experimental investigation on 4D printing of PET-G under bending, J. Mater. Res. Technol. 18 (2022) 2552–2569, https://doi.org/10.1016/J.JMRT.2022.03.121.
[24] E. Soleyman, M. Aberoumand, K. Soltanmohammadi, D. Rahmatabadi, I. Ghasemi, M. Baniassadi, K. Abrinia, M. Baghani, 4D printing of PET-G via FDM including tailormade excess third shape, Manuf. Lett. 33 (2022) 1–4, https://doi.org/10.1016/j.mfglet.2022.05.002.
[25] E. Soleyman, D. Rahmatabadi, K. Soltanmohammadi, M. Aberoumand, I. Ghasemi, K. Abrinia, M. Baniassadi, K. Wang, M. Baghani, Shape memory performance of PETG 4D printed parts under compression in cold, warm, and hot programming, Smart Mater. Struct. 31 (2022) 085002, https://doi.org/10.1088/1361-665X/AC77CB.
[26] S. Wachirahuttapong, C. Thongpin, N. Sombatsompop, Effect of PCL and compatibility contents on the morphology, crystallization and mechanical properties of PLA/PCL blends, Energy Proc. 89 (2016) 198–206, https://doi.org/10.1016/J.EGYPRO.2016.05.026.
[27] D. Rahmatabadi, I. Ghasemi, M. Baniassadi, K. Abrinia, M. Baghani, 3D printing of PLA-TPU with different component ratios: fracture toughness, mechanical properties, and morphology, J. Mater. Res. Technol. 21 (2022) 3970–3981, https://doi.org/10.1016/j.jmrt.2022.11.024.
[28] V.H. Sangeetha, T.O. Varghese, S.K. Nayak, Toughening of polylactic acid using styrene ethylene butylene styrene: mechanical, thermal, and morphological studies, Polym. Eng. Sci. 56 (2016) 669–675, https://doi.org/10.1002/PEN.24293.
[29] A. Chrysochoos, O. Arnould, Thermal and energy analysis of DMTA tests, J. Theor. Comput. Appl. Mech. (2023), https://doi.org/10.46298/JTCAM.9726.
[30] D. Rahmatabadi, M. Aberoumand, K. Soltanmohammadi, E. Soleyman, I. Ghasemi, M. Baniassadi, K. Abrinia, M. Bodaghi, M. Baghani, Toughening PVC with biocompatible PCL softeners for supreme mechanical properties, morphology, shape memory effects, and FFF printability, Macromol. Mater. Eng. (2023) 2300114, https://doi.org/10.1002/MAME.202300114.
[31] M.G.J. Waters, R. Jagger, K. Williams, V. Jerolimov, Dynamic mechanical thermal analysis of denture soft lining materials, Biomaterials 17 (1996) 1627–1630, https://doi.org/10.1016/0142-9612(95)00330-4.
[32] D.T.H. Wong, H.L. Williams, Dynamic mechanical and vibration damping properties of polyurethane compositions, J. Appl. Polym. Sci. 28 (1983) 2187–2207.
[33] M.M. Caruso, D.A. Davis, Q. Shen, S.A. Odom, N.R. Sottos, S.R. White, J.S. Moore, Mechanically-induced chemical changes in polymeric materials, Chem. Rev. 109 (2009) 5755–5798, https://doi.org/10.1021/CR9001353/ASSET/CR9001353.FP.PNG_V03.
[34] J.D. Badia, L. Santonja-Blasco, A. Martínez-Felipe, A. Ribes-Greus, Dynamic mechanical thermal analysis of polymer blends, Charact. Polym. Blends Miscibility, Morphol. Interfaces (2015) 365–392, https://doi.org/10.1002/9783527645602.CH12, 9783527331.
[35] R.P. White, J.E.G. Lipson, Polymer free volume and its connection to the glass transition, Macromolecules 49 (2016) 3987–4007, https://doi.org/10.1021/ACS.MACROMOL.6B00215/SUPPL_FILE/MA6B00215_SI_001.PDF.
[36] C.G. Robertson, C.M. Roland, Glass transition and interfacial segmental dynamics in polymer-particle composites, Rubber Chem. Technol. 81 (2008) 506–522, https://doi.org/10.5254/1.3548217.
[37] J. Suhr, N.A. Koratkar, Energy dissipation in carbon nanotube composites: a review, J. Mater. Sci. 43 (2008) 4370–4382, https://doi.org/10.1007/S10853-007-2440-X/METRICS.
[38] M. Sahihi, F. Bedoui, Nano-Reinforced Polymers and Polymer Nanocomposites, 2024, pp. 267–287, https://doi.org/10.1007/978-981-99-7848-9_13.
[39] R. Singh, R. Kumar, I.S. Ahuja, Thermal Analysis for Joining of Dissimilar Polymeric Materials through Friction Stir Welding, 2017.
[40] K.P.M. Lee, M. Brandt, R. Shanks, F. Daver, Rheology and 3D printability of percolated graphene–polyamide-6 composites, Polymers (Basel) 12 (2020) 2014.
[41] H.P. Schreiber, A. Rudin, Effect of carbon black on time dependence of the melt flow index, J. Appl. Polym. Sci. 11 (1967) 1043–1053.
[42] A. Shenavar, F. Abbasi, M.K.R. Aghjeh, A. Zamani, Flow and mechanical properties of carbon black filled acrylonitrile-butadiene-styrene (ABS), J. Thermoplast. Compos. Mater. 22 (2009) 753–766.
[43] L. Xia, H. Gao, W. Bi, W. Fu, G. Qiu, Z. Xin, Shape memory behavior of carbon black-reinforced trans-1,4-polyisoprene and low-density polyethylene composites, Polymers 811 (2019) 807, https://doi.org/10.3390/POLYM11050807, 2019, Vol. 11, Page 807.